International Journal of Nanoelectronics and Materials
IJNeaM
ISSN 1985-5761 | E-ISSN 2232-1535

Characterization of Nanocrystalline SnS Thin Film Fabricated used PLD Method for Photodetection Applications

Suad M.Kadhim

Laser and Optoelectronics Engineering Department, University of Technology- Iraq.
Corresponding author: Suad.M.Kadhim@uotechnology.edu.iq

Received 25 October 2023 & Accepted 12 December 2023

ABSTRACT

Pulsed laser deposition was used to create tin sulfide (SnS) nanoparticles with a Nd:YAG laser (700 mJ) with laser pulses of (200, 250, 300, and 350 pulses). Nanoparticles were created and investigated using XRD, AFM, and UV-Vis spectroscopy to understand their optical, topographical, and electrical properties. After that, a SnS photodetector was built for the first time, and its performance, photoresponse, and sensitivity were evaluated. The development of monocrystalline SnS films was confirmed by X-ray diffraction (XRD) examination. Clear crystallization with increased crystalline size and the optimum orientation was observed in the sample synthesized SnS thin film treated with 300 pulses. The crystallite size increased from 44 at 200 to 77 nm for 350 pulses. These films were characterized by better surface morphology with (111) preferred crystals. In addition, atomic force microscopy (AFM) studies showed that the average diameter of generated SnS nanoparticles rose from (39.4 nm to 64.7) nm when the laser pulses increased in pulsed laser deposition. Transmission measurements were used to determine the films' absorption coefficient energy gap (Eg), and they showed that the optical transition was direct and that the transmittance value dropped with increasing laser pulses. Band gap energy is reduced from 2.139 to 1.773 eV. Moreover, Hall Effect measurements on all samples demonstrate that all thin films were n-type, with charge carrier concentration increasing with increased pulses and carrier mobility decreasing with increased pulses. The photodetectors ' photosensitivity was evaluated in the dark after depositing Al contacts on SnS thin films through a metal mask. The Pulses of enhancement cause a red shift in the values of particular detectivity and quantum efficiency. The highest responsivity was obtained at 350 pulses, 6.72×10^{-1} AW^{-1}. The high (QE) of 150% at 200 p and detectivity of 2.9×10^{11} cm, $Hz^{1/2}.W^{-1}$ at 300p.

Keywords: *SnS, Thin films, photodetection, PLD, Structural, Optical.*

1. INTRODUCTION

Group IV-VI semiconductors have recently become important due to their suitable properties in many photoelectric, thermoelectric, and optoelectronic device applications [1]. The ability of sulfur salts in potential devices includes photovoltaics, thermoelectrics, catalysis, and cryogenic electronics. [2]. Due to the widespread application of image detectors in fields including optical imaging, optoelectronic circuits, and space communications, their preparation has garnered much attention [3]. UV light detectors have been made using various inorganic semiconductor materials, including CdS, ZnS, InSe, CdSe, and metal oxide semiconductors, including ZnO, CeO_2, and V_2O_5 [4]. The low optical band gap and favourable optoelectronic features of group IV-VI semiconductors are well known [5]. In the visible spectrum, tin sulfide (SnS) has a high absorption coefficient ($\alpha > 10^4$ cm^{-1}) [6]. In contrast to the heavy metal compounds (cadmium, mercury, lead) that are currently utilized in detector applications, it has a low toxicity. SnS has chemical stability, and the elements that enter into its composition are cheap and widely available. SnS has an orthogonal structure of layers. Polycrystalline SnS thin films have a direct energy gap of (1.27-1.5 eV), while single-crystal SnS thin films have an indirect energy gap of 1.1 eV [7]. Tin sulfide's useful physical qualities have led to its widespread use across a wide range of industries, such as photovoltaics [8], photoconductors [9], gas sensors [10], and photocatalysis [11], solar cells [12]. SnS films for light detectors can be deposited using a variety of methods, including co-evaporation [13], chemical bath deposition (CBD), sputtering [14], vacuum evaporation [15], physical vapour deposition [16], etc. The pulsed laser deposition method is one such method, as this technique has the advantages of high purity, compact shape, homogeneity, and regularity, in addition to the high deposition rate. Because of this, in the present research, the PLD method was used to develop SnS thin films for photodetector application.

2. MATERIAL AND METHODS

Quartz substrates and silicon wafer are adopted for the prepared thin film utilizing the pulsed laser deposition (PLD). They had a resistivity of roughly (1- 5) Ω and a p-type (111) orientation, and the thickness was (500±10) μm. The chemical and ultrasonic methods were adopted to clean the quartz substrates, the ethanol and distilled water were used to clean the substrate. Then, the samples were placed in a beaker containing distilled water inside the ultrasound machine for 2 hours. The etching treatment removed the top layer (native oxide) of silicon. The

powder SnS was compressed by a single compression tool at a pressure of 160 kg, and the samples were compressed in disks at a diameter of 1cm and thickness of 3 mm, and the substrates and target were fixed in the chamber of the PLD system. The pulsed laser deposition system with base energy of laser of 800 mJ, the frequency of laser (10 Hz) and the number of pulses change from (200–350 pulses), and the deposition chamber pressure is kept at 10^{-4} Torr. The prepared thin film's thickness was obtained by Fizeau optical interference [15] equipped with a He-Ne laser source and a beam expander. The following was used to calculate the thickness of each prepared film:

$$t = \frac{\lambda}{2}.\frac{\Delta x}{x} \quad (1)$$

To illustrate this, let us say that x represents the length of the visible fringe, and Δx represents the spacing between adjacent fringes. The essential properties of the SnS films were considered by (XRD) using a Rigaku D MAX-2000 powder diffractometer engaging Cu Kα radiation (0.15 = 0.154056 nm) with 2θ in the range (20°–70°). To determine the typical crystal size, Scherer's formula was applied [17]:

$$G.S = \frac{A\lambda}{\cos\theta\Delta\theta} \quad (2)$$

where D is the typical size of a crystallite (grain), a constant K is (~1), the wavelength is λ, β is (FWHM) the full width at half maximum of the XRD peaks, and θ is the Bragg angle. AFM produces 3D images to describe surface morphology (TT-2 Workshop Company, United Sta. The transmission and absorbance spectrum of SnS films /quartz in the range (400-1100 nm) were measured using a Cecile CE 7200 Spectrophotometer. The absorption coefficient (α) of the films can be calculated using the transmission spectrum data, as shown in Equation (3) [18]:

$$\alpha = \frac{1}{d}\ln\frac{1}{T} \quad (3)$$

where *T* represents the transmittance and *d* represents the thickness of such film.
The following equation is used to find out the energy gap values of the tin sulfide films [18]:

$$\alpha h\nu = A(\mathrm{h}\nu - \mathrm{Eg})^{0.5} \quad (4)$$

The Hall Effect was used to study the electrical properties of SnS thin films, allowing researchers to learn more about the mobility and concentration of charge carriers in the material. Using a mask and heat evaporation, an Al electrode was placed on the surface of the samples. Electric current requires a potential difference (as measured by the Ministry of Science and Technology) to flow through a thin layer.

The Dark current–voltage SnS/Si measurements were studied using a power source (China, Dazheng, 30 V, 5 A, PS-305D), applying a potential difference of (5 to -5). The measurements were taken with a Halogen lamp providing light at 80mW/cm^2 and a power meter calibrated with silicon measuring the intensity of the lamp's light. A programmable LCR meter (Taiwan: GW INSTEK LCR-6100, 10 Hz-100 kHz) was used to determine its amplitude and voltage characteristics. Potential ranged from 0 to 3 V, with the total film voltage dictated by the location on the curve where $1/C^2$ equals 0. A monochrometer covering the wavelength range of (200-1000) nm was used to evaluate the spectral responsiveness of the SnS/Si junction.
Calibration of the power was done with a silicon power meter. The following equations are used to compute the responsivity R, directivity D* and quantum efficiency [19]:

$$R_\lambda = \frac{I_{ph}}{P} \quad (5)$$

$$D^*_\lambda = \frac{I_{ph}}{I_n}\sqrt{A\Delta f} \quad (6)$$

where In is the noise current given by In=√(2qI$_d$, A is the area of the detector, Δf is the frequency, and Id is the dark current [20] :

$$\eta = \frac{Rhc}{\lambda} \quad (7)$$

3. RESULTS AND DISCUSSION

The wafer's electrical and optical properties might be affected; hence, measuring thin film thickness is important. Figure 1 displays the results of measuring the thickness of the thin films by applying equation (1) to all samples. The PLD method selectively removes larger particles from the target surface and deposits them on the substrates. As the laser pulses increase, the resulting film thickness also increases. Increasing the laser pulses to 250p showed an increase in the obtained film's thickness to about 110nm. Further increasing the laser pulses to 300 and 350p showed a significant increase in each film's thickness. The thickness changes from (83 to 155 nm), and the maximum thickness of the films is 155 nm at 350 pulses.

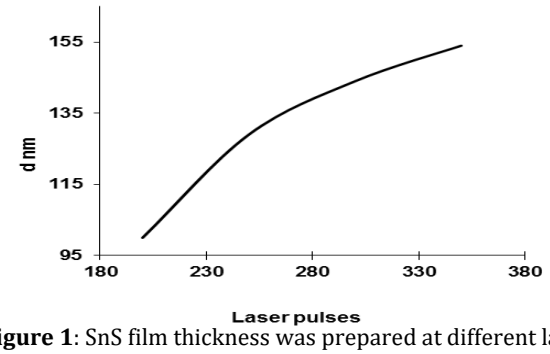

Figure 1: SnS film thickness was prepared at different laser pulses.

The XRD patterns of SnS films for a range of laser pulses (200-350p) are shown in Figure 2. We notice no impurity phases such as SnS, SnS2 and Sn2S3 polymorphs. It was observed through X-ray diffraction that the diffraction peaks of the prepared films have orthorhombic crystalline structures. The profiles contain four peaks corresponding to the planes (120), (021), (101) and (111), respectively. As the laser pulse was increased to 350p, the film's aligned crystals provided the optimal crystal orientation for the diffraction peak (111). The apex (111) gradually becomes more intense. Based on the findings, it was determined that laser pulses play a significant role in establishing the phase and purity of SnS films. The crystallite size (G.S.) was determined using Equation (2). A higher laser pulse (up to 350p) achieved higher crystallinity. Crystallite size increased from (44.3 to 77.4nm). The crystalline size of films increases as they rise pulses of 350p [21].

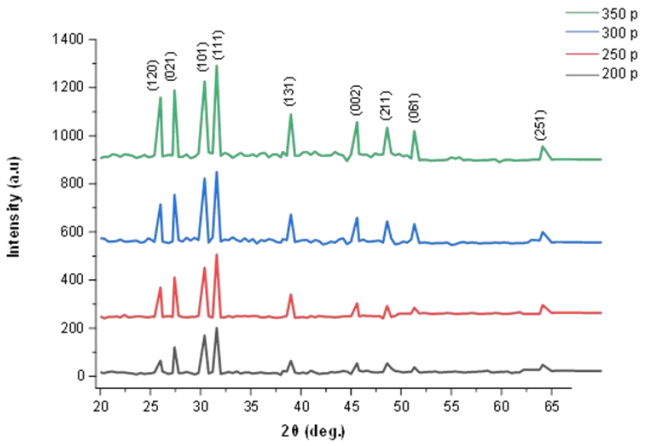

Figure 2: X-ray patterns of SnS films at various laser pulses.

The atomic force microscopy (AFM) surface pictures of thin films generated at different laser pulses are shown in Figure 3. When the number of pulses was 200p, the surface was irregular, and the particle distribution was not homogeneous. We notice that the shapes of the particles are different; some are spherical, and some are rods. When the number of pulses increased to 300, we noticed that the surface became homogeneous and possessed a high degree of regularity. The particles are approximately spherical [22]. The surface became more homogeneous, the particles were arranged with high regularity, and a clear protrusion prevailed over the entire surface when the number of pulses increased to 350. The roughness of nanostructure films changes as the laser pulses change. The roughness of the films Ra was (25.56nm to 56.88) nm, and Rq was (34.72 - 46.81) nm, and it increases when the laser pulses rise from (200p to 350p). Table 1 displays the average grain size, root mean square, and roughness of films made using a variety of laser pulses.

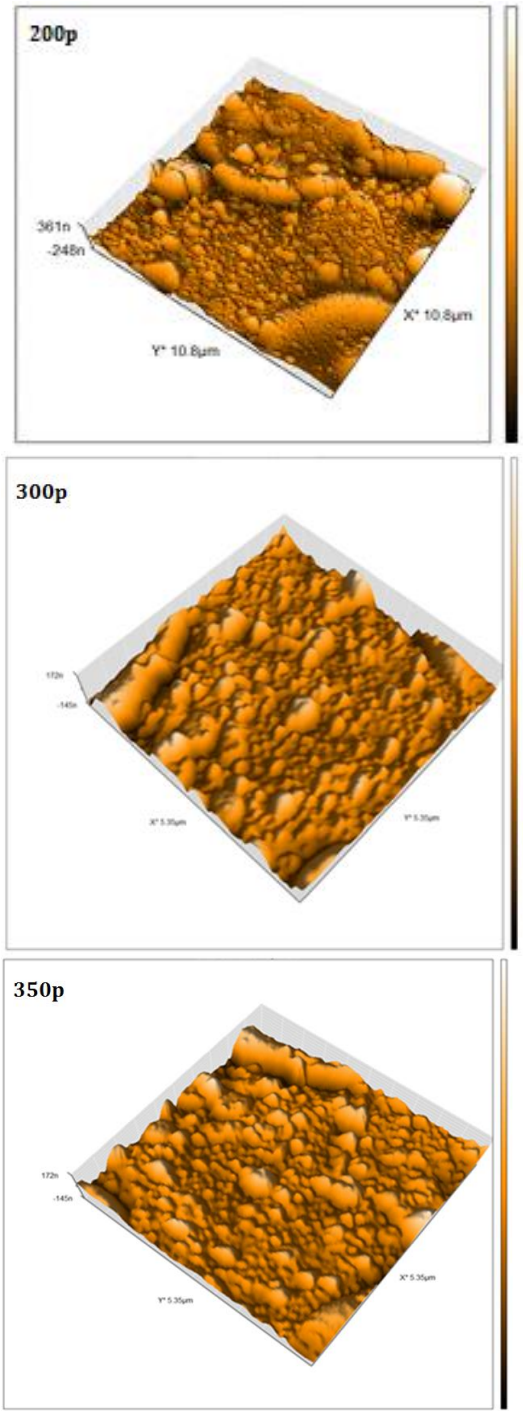

Figure 3: AFM image of nano SnS at different laser pulses.

Table 1: Nanostructure parameters of AFM image of SnS films.

Laser pulses	Average grain size (nm)	Average roughness (nm)	Root mean square (nm)	Grain size (nm)(x-ray)
200	39. 4	25.56	34.7	44.3
300	51.5	34.47	39.5	60.8
350	64.7	56.88	46.8	77.4

Figure 4 displays the optical transmittance spectra of SnS thin films subjected to different laser pulses between (200p) and (350p), between 400 and 1100 nanometers in length. All films were found to have an increasing transmittance with increasing wavelength. Increasing the pulses from 200p to 350p causes a decrease in transmission, as shown by the spectra. Light absorption increases, leading to more electronic transitions between the valence and conduction bands, which causes this effect [23]. Observed at the longer wavelength range, as shown in the Figure, the transmittance spectrum showed distinct interference fringes, proving the film's thickness uniformity by reflecting light from both sides.

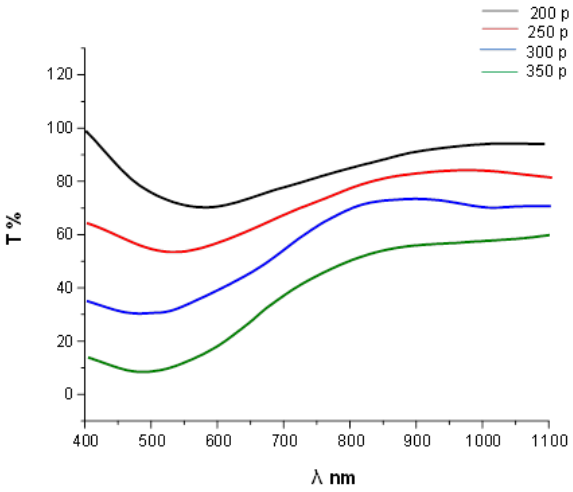

Figure 4: Optical transmittance spectra.

Figure 5 is a plot showing the dependence of the optical absorption spectra on laser pulse for the SnS nanoparticles produced by a 1064 nm laser (200, 250, 300, 350p). There was a noticeable change in the optical absorption of SnS nanoparticles toward the 400 nm wavelength. As the pulses grew longer, the particles expelled from the target grew larger and absorbed more energy. Due to the larger kinetic energy of the expelled particles, there were more states in which photons could be absorbed, leading to a higher density of particles [24]. All of the deposited films had strong absorption in the visible range due to the fit state between them, and we observed improved absorption due to the enhanced band-to-band transition.

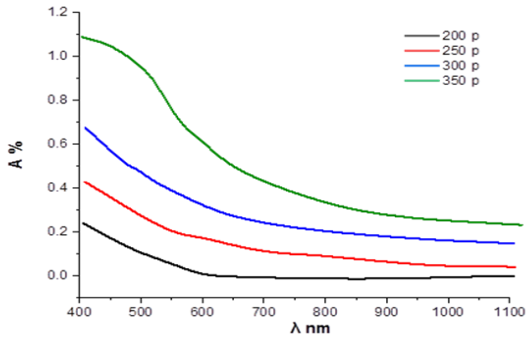

Figure 5: Optical absorption spectra.

As the ability of a substance to absorb light of a specific wavelength, the absorption coefficient (α) is measured in terms of the reciprocal of distance. The absorption coefficient (α) was determined using Equation (3). As seen in Figure 6, the absorption coefficient rises alongside the laser pulses. In the visible spectrum, between 400 and 550 nm, the films exhibit a markedly high absorption coefficient, then gradually diminish depending on the film's structure, eventually leveling off at long wavelengths (>750 nm), where, at this wavelength, the films are completely transparent. All SnS films were found to have an absorption coefficient in the order of $10^5 cm^{-1}$ above the fundamental absorption edge.

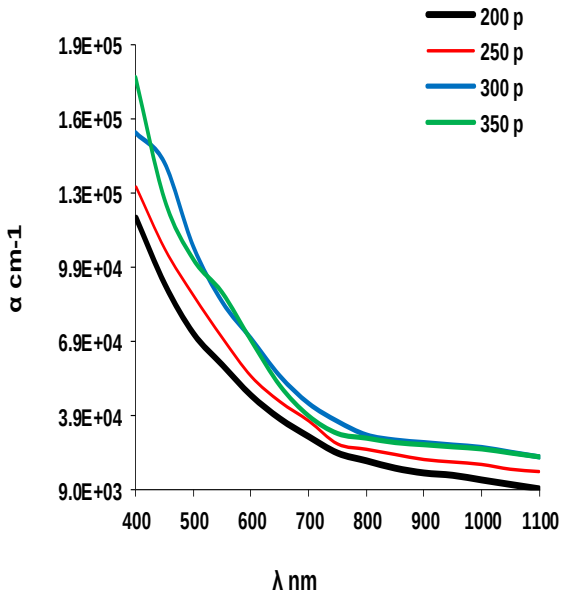

Figure 6: Absorption coefficient of SnS thin films with laser pulses.

The crystal structure, atomic distribution, and crystal regularity are important factors in determining film energy gap values [25]. From the graph of $(\alpha h\nu)^2$ versus photon energy (hν), the values of the direct energy gap (Eg) are figured out, as depicted in Figure 7. The direct band gap range (1.773, 1.901, 1.827, and 2.139 eV) was calculated. From Equation (4) for SnS, thin films of various laser pulses of 200, 250, 300, and 350p are comparable with other values reported for SnS orthorhombic. It can be noted that the Eg decreases with the increase in the number of pulses up to 250 pulses. When reaching 300 pulses, the Eg value increases. Once the pulse count reaches 350, however, the Eg starts to drop again, which may result from improved crystallinity and/or a thicker film. At the same time, the band gap grows as lead ion concentration rises due to smaller grains and weaker quantum confinement [26].

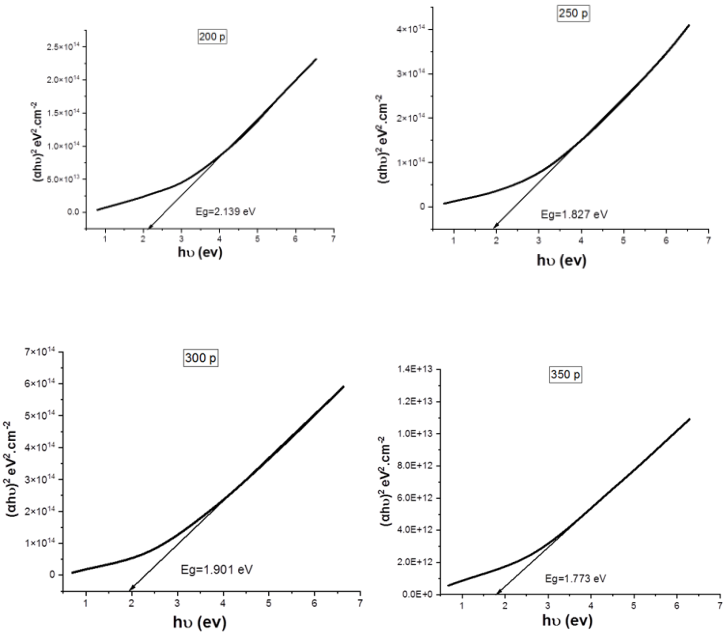

Figure 7: The energy gap of SnS nanostructured films with different laser energy.

To assess some of the electrical characteristics of the SnS thin film, hall measurements have been made. Hall Effect measurements were utilized to identify the charge carrier concentration (C.C), mobility (μ_H), and semiconducting kinds of the SnS thin films produced using a variety of laser pulses. Every single film was n-type. Figure 8 and Table 2 display the relationship between C.C, μ_H conductivity, and laser pulses. By doubling the laser pulse duration from 200 p to 350 p, the concentration of charge carriers jumped from 6.23 x 10^{16} to 12.8 x 10^{16} cm^{-3}. This is caused by a drop in sulfide vacancies, the material's primary source of charge carriers; however, as the number of laser pulses is increased, the scattering caused by the increasing lattice defects causes the charge carrier mobility to fall from (300 to 86.8) cm^2/V.s. These findings could be explained by increased average grain size due to exposure to laser pulses [27].

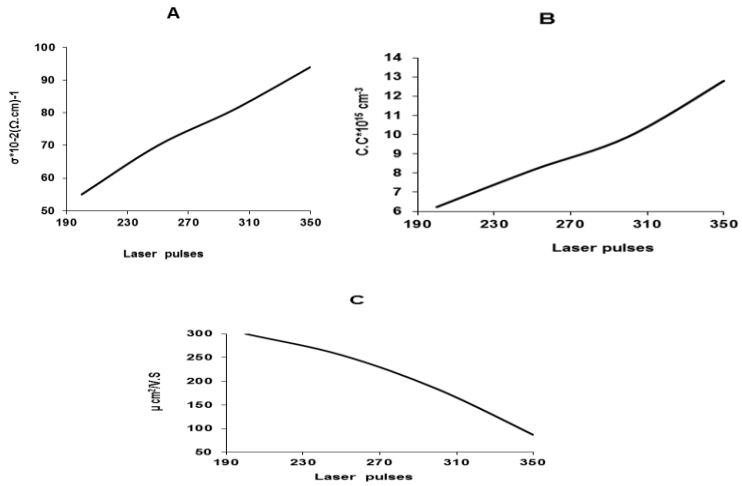

Figure 8: variation of A) conductivity, B) concentration, and C) mobility with the laser energy.

Table 2: Hall Effect Measurements for SnS thin films prepared by PLD.

Laser pulses	R_H ($cm^{-3}C^{-1}$)×10^3	C.C ($cm)^{-3}$×10^{16}	σ*10-^{2}(Ω.cm)$^{-1}$	μ (cm^2V^{-1}/s)
200	-10.31	-6.23	55.2	300
250	-8.24	-8.18	70.6	255.2
300	-6.53	-9.89	81.4	183.4
350	-5.88	-12.8	94.7	86.8

It is an important technique generally used to study the electrical properties of any junction (homo or hetero). Figure 9 depicts the forward and reverse bias voltage I-V characteristics of a nano SnS/Si heterojunction for various laser pulses. The breadth of the depletion layer and the built-in potential decrease due to the forward dark current generated by the flow of majority carriers in regions where the applied voltage injects majority carriers. In the case of reverse bias, the generation current dominates, the diffusion current dominates, and the current somewhat increases with an increase in the applied voltage. This figure shows dark current-voltage properties of SnS prepared by PLD at pulses (200 to 350 p), at biases (5 to -5) and increased bias voltage due to decreased depletion layer width. Notably, the current increases dramatically at a forward bias voltage, while the current rises Battani with reverse voltage. And the current increases with increasing laser pulses.

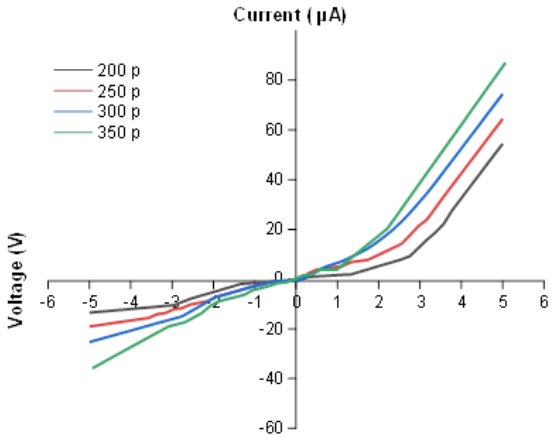

Figure 9. I-V characteristic of SnS/Si heterojunction at dark state.

The photocurrent is a very important parameter in photodetectors and greatly impacts the spectral responsivity and quantum efficiency. The I-V characteristic of 80 mW/cm^2 illuminated nano SnS/ Si at different laser pulses is depicted in Figure 10. The graph shows that the photocurrent rises as the bias voltage is raised. These findings may be associated with an increase in the concentration of photons detected where an internal electric field was extended as the width of the depletion layer increased [28]. Increases in both the depletion width and the number of photogenerated charge carriers that float within the depletion region and the diffusion carrier's region cause an increase in photocurrent density. This, in turn, reduces grain boundaries and improves the structure, subsequently increasing the mobility and the photocurrent

density, thus increasing the creation of electron-hole. From these results, the current values are increased proportionally with the presence of light due to the resistance changes.

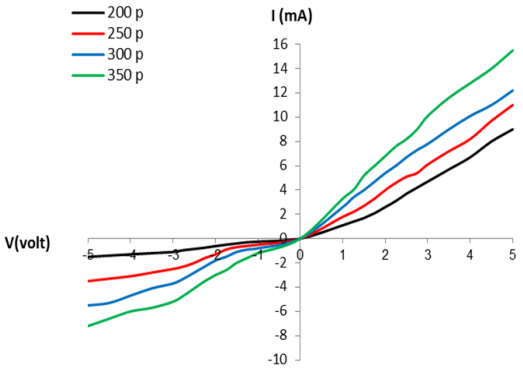

Figure 10. I-V characteristic of SnS/Si heterojunction at present light.

Figure 11 It represents the C-V characteristics of SnS films at different pulse numbers (200, 250, 300, and 350p) under (0 to –3 V) voltage. This figure depicts the variation of heterojunction capacity with reverse bias voltage. It was found that the capacitance dropped with increasing reverse bias voltage. The expanding depletion region is responsible for this behaviour by lowering the capacitance at the junction sides. It has also been observed that laser beam exposure decreases Vbi value because structural defects are repaired, and carrier concentration is increased, leading to a rise in capacitance [29].

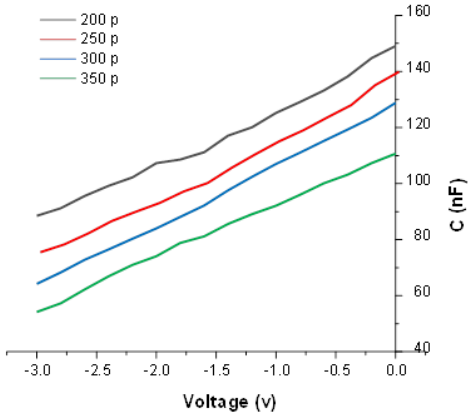

Figure 11. C-V characteristic of SnS/Si at various pulse numbers.

For samples prepared at different pulses, the square of the inverse capacitance at the SnS/Si heterojunction is shown in Figure 12, plotted against the reverse-bias voltage. The zero-point extrapolation of the linear portion of $1/C^2$ yielded the value of the built-in potential (Vbi). The laser pulses have caused an increase in the depletion layer, leading to a rise in the Vbi value of all heterojunctions [31]. Preparation of SnS/Si films resulted in voltages of 0.37, 0.67, 0.77, and 0.96eV due to the disparity between the width of the depletion region created by laser pulses during growth and the concentration of individual electrons in the nano SnS.

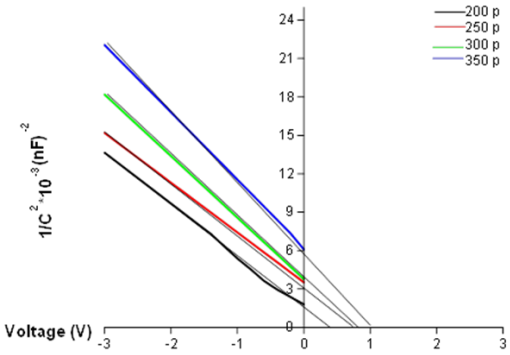

Figure 12. $1/C^2$-V characteristics of SnS/Si heterojunction at different laser pulses.

Spectral sensitivity is defined as the output current divided by the incident power. Figure 13 displays the predicted spectrum responsivity at 3V for SnS/Si heterojunctions generated with varying laser pulses at laser fluency 1064 nm and investigated in the (200-1000) nm wavelength range, which were calculated from Equation (5). The silicon substrate's absorption edge is apparent in the visible region, revealing the absorption edge of the SnS thin film layer. The short wavelength detection has mainly occurred at the region in the vicinity of the SnS thin film layer.

In contrast, long wavelength detection is carried out at the silicon depletion region. After increasing the laser pulses, the spectrum responsivity showed a little shift toward long wavelengths due to the fluctuation in the SnS energy gap. An incoming beam with energy greater than the energy band gap can stimulate electron-hole pairs, leading to a greater spectrum response [30]. There is a0.72A/W maximum peak in photosensitivity.

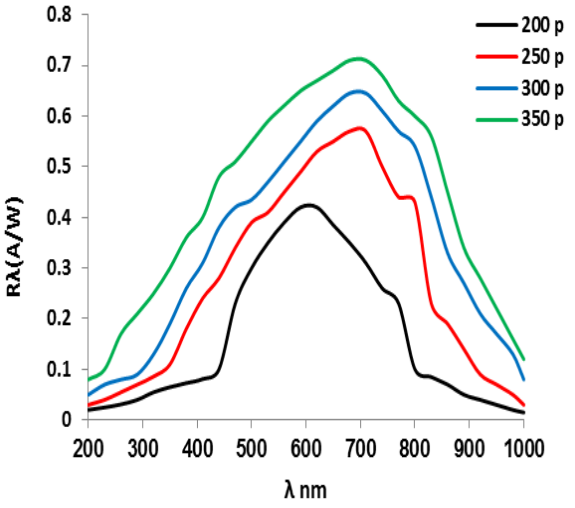

Figure 13. Responsivity setup for the SnS/Si heterojunction on different laser pulses.

Specific detectivity is the minimum incident power value that the detector can detect. Specific detection values were calculated according to Equation (6). Changes in specific detection (D*) with wavelength for SnS/Si heterojunctions at different laser pulses (200, 250, 300, and 350p) are shown in Figure 14. The specific detectivity plot is similar to that of the responsivity plot. It is evident that the specific detectivity D* increases with increasing laser pulses until it reaches 300 pulses due to decreased dark current, which reduces contribution to the noise current. Still, when the number of pulses reaches 350, the detection decreases slightly. It was the maximum value of the detection (2.85 x 10^{11} cm. Hz $^{1/2}$.W^{-1}) at 300 pulses. Enhanced photodetector detectivity may result from increased detector responsiveness, decreased structural defect concentration, and reduced leakage current [32].

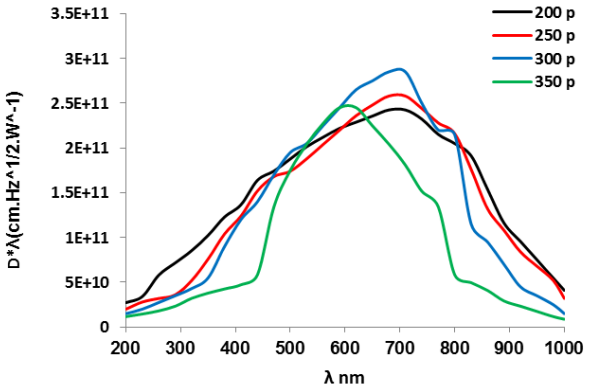

Figure 14. D* vs. wavelength for SnS/Si at various laser pulses.

Quantum efficiency (η) is a very important parameter for the detector because it represents the ratio between the heterogeneous excited electrons and the number of incident photons in the practical region, which is related to the responsivity according to Equation (7). Figure 15 shows the change of (η) with the wavelength of SnS/Si at different laser pulses (200, 250, 300, 350p). Figure 15 demonstrates how laser pulses reduce the maximum quantum efficiency. With longer laser pulses, the quantum efficiency drops. The maximum quantum efficiency in the UV region is (70.18%) at 200p.

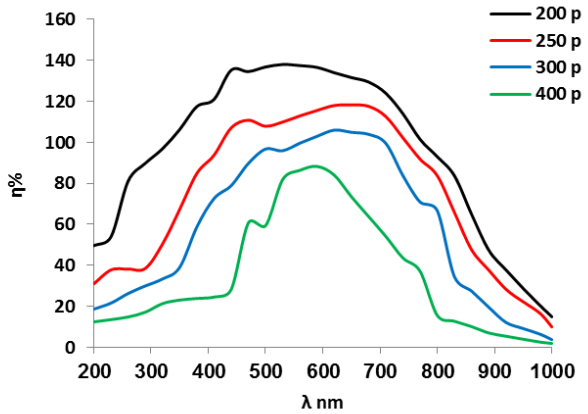

Figure 15. quantum efficiency vs. wavelength for SnS/Si heterojunction at various laser pulses.

Table 3: Shows the detectivity, quantum efficiency, responsivity, and energy gap value of SnS/Si heterojunction

.

Laser pulses	Rλ (A/W) sponsivety	Detectivity D*(cm.Hz $^{1/2}$.W^{-1})	Quantum Efficiency (η)(%)	Eg(eV)
200	0.42	2.42E+11	70.18%	2.139
250	0.57	2.58E+11	58.91%	1.827
300	0.64	2.85E+11	51.03%	1.901
350	0.71	2.45E+11	40.33%	1.773

4. CONCLUSION

Briefly, visible light photodetectors fabricated using SnS nanoparticles were synthesized by the PLD method. SnS films of various laser pulses changing from (200 to 350p) were used to manufacture optical detectors to investigate the effect of pulse number on photodetectors' performance. The SnS films were characterised by XRD, AFM, and a UV–Vis spectrometer. The maximum photodetector parameters such as Rλ, η, D*, showed higher values of 0.72 A/W, 70.18%, and 2.85*10^{11}cm.Hz$^{1/2}$.W^{-1}, respectively.

ACKNOWLEDGMENTS

All authors are thankful and Acknowledge all Laser and Optoelectronics Engineering Department, University of Technology, for supporting this research.

REFERENCES

[1] S.S. Hegde, A.G. Kunjomana, P. Murahari, B.K. Prasad, and K. Ramesh, "Vacuum annealed tin sulfide (SnS) thin films for solar cell applications," *Surf. Interfaces*, vol. 10, pp. 78–84, 2018.

[2] A. Javed, N. Khan, S. Bashir, M. Ahmad, and M. Bashir, "Thickness dependent structural, electrical, and optical properties of cubic SnS thin films," *Mater. Chem. Phys.*, vol. 246, p. 122831, 2020.

[3] K.D. Arun Kumar, P. Mele, M. Anitha, S. Varadharajaperumal, D. Alagarasan, N.S. Alhokbany, T. Ahamad, and S.M. Alshehri, "Simplified chemical processed Cd1-xAlxS thin films for high-performance photodetector applications," *J. Phys. Condens. Matter*, vol. 33, p. 195901, 2021.

[4] D. Alagarasan, S.S. Hegde, S. Varadharajaperumal, R. Aadhavan, R. Naik, Mohd Shkir, H. Algarni, and R. Ganesan, "Effect of SnS thin film thickness on visible light photo detection," *Phys. Scr.*, vol. 97, p. 065814, 2022. DOI: 10.1088/1402-4896/ac6d19

[5] S. Kawanishi, I. Suzuki, S.R. Bauers, A. Zakutayev, H. Shibata, H. Yanagi, and T. Omata, "SnS homojunction solar cell with n-type single crystal and p-type thin film," *Sol. RRL*, vol. 5, p. 2000708, 2021.

[6] Y. Iguchi, K. Inoue, T. Sugiyama, and H. Yanagi, "Single-crystal growth of Cl-doped n-type SnS using SnCl2 self-flux," *Inorg. Chem.*, vol. 57, p. 6769, 2018.

[7] A. Gḿez, H. Martinez, M. Calixto-Rodrىguez, D. Avellaneda, P.G. Reyes, and O. Flores, "A Study of the

Structural, Optical and Electrical Properties of SnS Thin Films Modified by Plasma," *J. Mater. Sci. Eng. B*, vol. 3, no. 6, pp. 352–358, 2013.

[8] H. Martinez and D. Avellaneda, "Modifications in SnS Thin Films by Plasma Treatments," *Nucl. Instrum. Methods Phys. Res.*, vol. 272, pp. 351–356, 2012.

[9] C. Gao, H. Shen, L. Sun, and Z. Shen, "Chemical Bath Deposition of SnS Films with Different Crystal Structures," *Mater. Lett.*, vol. 65, pp. 1413–1415, 2011.

[10] J. Henry, K. Mohanraj, S. Kannan, S. Barathan, and G. Sivakumar, "Structural and Optical Properties of SnS Nanoparticles and Electron-Beam Evaporated SnS Thin Films," *J. Exp. Nanosci.*, vol. 10, no. 2, pp. 78–85, 2015. DOI: 10.1080/17458080.2013.788226

[11] B.A. Hasan and I.H. Shallal, "Structural and Optical Properties of SnS Thin Films," *J. Nano. Adv. Mat.*, vol. 2, no. 2, pp. 43–49, 2014.

[12] S. Al-Jawad, M.R. Mohammad, and N.J. Imran, "Effect of Electrolyte Solution on Structural and Optical Properties of TiO2 Grown by Iodization Technique for Photoelectrocatalytic Application," *Surf. Rev. Lett.*, vol. 25, p. 1850078, 2018.

[13] Z.D. Yasmeen, "Study the Effect of Laser Energy Change on Optical and Properties of Fe2O3 Thin Films Deposited by PLD Technique," *ARPN J. Eng. & App. Scie.*, vol. 16, no. 12.

[14] M.K. Suad, "Effect of Deposition Parameters on Kinematics Growth and Optical Properties of Fe2O3 Nano Films Deposited by PLD," *J. Made. Alel. Coll.*, vol. 11, no. 1.

[15] D.F. Abulqader, A.A. Ali, and K.K. Wafaa, "Photodetector Fabrication Based on Heterojunction of CuO/SnO2/Si Nanostructures," *Bul. of Mat. Sci.*, vol. 45, no. 84. DOI: 10.1007/s12034-022-02672-x

[16] G. Evgeny, S. Dmitry, T. Tatyana, I. Vladimir, K. Sergey, M. Aleksandr, N. Aleksey, and U. Dmitry, "Spray Pyrolysis Deposited Cr and In Doped CdS Films for Laser Application," *Opti. Mate.*, vol. 117, p. 111153, 2021.

[17] Z.D. Yasmeen, "Influence Optical and Morphology Properties of Films (CdS) Prepared by Pulse Laser Deposition (PLD) Technique," *Inter. J. Nanoelectr. & Mat.*, vol. 15, no. 1, p. 1, 2022.

[18] T.K. Pathak, J.K. Rajput, V. Kumar, L.P. Purohit, H.C. Swart, and R.E. Kroon, "Transparent Conducting ZnO-CdO Mixed Oxide Thin Films Grown by the Sol-Gel Method," *J. Coll. Interf. Sci.*, vol. 487, p. 378, 2017.

[19] D.F. Abulqader, A.A. Ali, and K.K. Wafaa, "Photodetector Fabrication Based on Heterojunction of CuO/SnO2/Si Nanostructures," *Bul. of Mat. Sci.*, vol. 45, no. 84. DOI: 10.1007/s12034-022-02672-x

[20] Tejendra D, Akash T, Swanand VS, K.L. Ganapathi, and Ramachandra M.S., "Ultra-Wide Bandgap Copper Oxide: High Performance Solar-Blind Photo-detection," *IEEE Electron Device Lett.*, vol. 41, no. 12, pp. 1790–1793, 2020. DOI: 10.1109/LED.2020.3030641

[21] R.A. Ismail, K.I. Hassan, O.A. Abdulrazaq, and W.H. Abode, "Optoelectronic Properties of CdTe/Si Heterojunction Prepared by Pulsed Nd:YAG-Laser Deposition Technique," *Mater. Sci. Semicond. Process.*, vol. 10, no. 1, pp. 19–23, 2007.

[22] R.A. Ismail, N. Hasan, and S.S. Shaker, "Preparation of Bi2Sr2CaCu2Ox Thin Film by Pulsed Laser Deposition for Optoelectronic Devices Application," *Silicon*, vol. 14, no. 6, pp. 2625–2633, 2022.

[23] S.H. Xu, J.Y. Huang, G.T. Fei, Y.S. Wei, L.G. Yuan, and B. Wang, "Sol-Gel Preparation of High Transmittance of Infrared Antireflective Coating for TeO2 Crystals," *Infrared Phys. Technol.*, vol. 118, p. 103881, 2021. DOI: 10.1016/j.infrared.103881

[24] A.J. Haider, T. Alawsi, M.J. Haider, B.A. Taha, and H.A. Marhoon, "A Comprehensive Review on Pulsed Laser Deposition Technique to Effective Nanostructure Production: Trends and Challenges," *Opt. Quantum Electron.*, vol. 54, no. 8, pp. 488, 2022

[25] M.A.M. Hassan, M.F.H. Al-Kadhemy, and E.T. Salem, "Effect Irradiation Time of Gamma Ray on MSISM (Au/SnO2/SiO2/Si/Al) Devices Using Theoretical Modeling," *Int. J. Nanoelectronics and Materials*, vol. 8, no. 2, pp. 69–82, 2014.

[26] M. Hassan, M. Fakhri, and S. Adnan, "2-D of Nano Photonic Silicon Fabrication for Sensing Application," *Digest J. Nanomater. Biostruct.*, vol. 14, no. 4.

[27] D. Yang and D. Ma, "Development of Organic Semiconductor Photodetectors: From Mechanism to Applications," *Adv. Opt. Mater.*, vol. 7, no. 1, pp. 1–23, 2019. DOI: 10.1002/adom.00522

[28] H. Kim et al., "Effect of Film Thickness on the Properties of Indium Tin Oxide Thin Films," *J. Appl. Phys.*, vol. 88, no. 10, pp. 6021–6025, 2000. DOI: 10.1063/1.1318368

[29] A.M. Mousa, S.M. Hassen, and S. Mohmoed, "Effect of Deposition Parameters on Kinematics Growth and Optical Properties of PbS Nano Films Deposited by Chemical Bath Deposition," *Int. Lett. Chem. Phys. Astron.*, vol. 34, no. 1, pp. 1–10. DOI: 10.18052/www.scipress.com/ilcpa.34.1

[30] Z. Fan et al., "Photoluminescence and Polarized Photodetection of Single ZnO Nanowires," *Appl. Phys. Lett.*, vol. 85, no. 25, pp. 6128–6130, 2004. DOI: 10.1063/1.1841453

[31] J.S. Jie, W.J. Zhang, Y. Jiang, X.M. Meng, Y.Q. Li, and S.T. Lee, "Photoconductive Characteristics of Single-Crystal CdS Nanoribbons," *Nano Lett.*, vol. 6, no. 9, pp. 1887–1892, 2006. DOI: 10.1021/nl060867g

[32] S. Ullah, A. Bouich, H. Ullah, B. Mari, and M. Molars, "Comparative Study of Binary Cadmium Sulfide (CdS) and Tin Disulfide (SnS2) Thin Buffer Layers," *Sol. Energy*, vol. 208, pp. 637–642, 2020.